RESEARCH ARTICLE

Microbial diversity and biomineralization in low-temperature hydrothermal iron–silica-rich precipitates of the Lau Basin hydrothermal field

Jiangtao Li[1], Huaiyang Zhou[1], Xiaotong Peng[1], Zijun Wu[1], Shun Chen[1] & Jiasong Fang[1,2]

[1]State Key Laboratory of Marine Geology, Tongji University, Shanghai, China; and [2]Department of Natural Sciences, Hawaii Pacific University, Kaneohe, HI, USA

Correspondence: Huaiyang Zhou, School of Ocean and Earth Science, Tongji University, Shanghai 200092, China. Tel.:+86 21 65983385; fax: +86 21 65987615; e-mail: zhouhy@tongji.edu.cn

Received 24 September 2011; revised 11 March 2012; accepted 13 March 2012. Final version published online 18 April 2012.

DOI: 10.1111/j.1574-6941.2012.01367.x

Editor: Christian Griebler

Keywords
iron-oxidizing bacteria; microbial mineralization; silicification; CDE hydrothermal field.

Abstract

Iron–silica-rich low-temperature hydrothermal precipitates were collected from the CDE hydrothermal field located at the East Lau Spreading Center. Phylogenetic analysis showed that the precipitates were dominated by the members of α-proteobacteria and marine group I archaea. Ultrastructural analysis suggested the bacteriogenic origin of the iron–silica-rich deposits. Distinctive biosignatures detected included straight filaments, helical stalks and curved irregular filaments, which were similar in appearance to those structures excreted by the known iron-oxidizing genera *Leptothrix* spp., *Gallionella* spp. and *Mariprofundus* spp. 16S rRNA gene analysis confirmed the presence of neutrophilic iron-oxidizing bacteria with the detection of phylotypes clustering with *Gallionella* spp. and the proposed ζ-proteobacteria class. Mineralogy and bulk geochemical analyses showed that the precipitates were dominated by amorphous silica with low amounts of iron. Based on microbiological, geochemical and mineralogical analyses, we conclude that silicification was a common process and microbial cells and related ultrastructures likely acted as nucleation templates for silica precipitation in the CDE hydrothermal field.

Introduction

Iron–silica-rich precipitates, generally formed in association with low-temperature hydrothermal fluids, have been commonly found in hydrothermal fields along mid-ocean ridges and back-arc spreading centres (Alt, 1988; Emerson & Moyer, 2002; Kennedy *et al.*, 2003; Davis *et al.*, 2009; Hodges & Olson, 2009; Peng *et al.*, 2011). Morphological evidence indicates that microorganisms play important roles in the formation of these mineral deposits (Juniper & Fouquet, 1988; Langley *et al.*, 2009 and references cited therein). Iron–silica precipitates usually exhibit unique micro-textures that are remarkably similar to microbial forms and are regarded as apparent bacterial origin. Ultrastructure analyses reveal that amorphous silica or Fe-oxyhydroxides aggregate on the outer surface of microorganism-like structures or completely replace original microbial cells by intracellular mineralization (Fortin *et al.*, 1998; Peng *et al.*, 2007). Particularly, putative Fe-oxidizing bacteria (FeOB) biosignature remains, such as filaments, sheaths and helical stalk-like morphologies are widely identified from these iron–silica deposits (Hrischeva & Scott, 2007; Templeton *et al.*, 2009; Edwards *et al.*, 2011).

However, direct evidence from microbial and molecular analyses in association with microbial mineralization has been limited. Although previous investigations using cultivation and molecular techniques to assess microbial communities have been carried out and novel FeOBs have been isolated (Emerson & Moyer, 2002; Emerson *et al.*, 2007), most of the studies focused primarily on dense iron-rich flocculent microbial mats at Loihi Seamount, Hawaii (Moyer *et al.*, 1995; Emerson & Moyer, 2002; Rassa *et al.*, 2009; Edwards *et al.*, 2011), Cleft Segment of Juan de Fuca Ridge (Davis *et al.*, 2009), Tonga-Kermadec Arc(Hodges & Olson, 2009; Forget *et al.*, 2010) and Southern Mariana Trough (Kato *et al.*, 2009). In contrast, direct microbiological and mineralogical evidence is still

lacking for low-temperature hydrothermal deposits that are composed mostly of amorphous silica with minute amounts of iron, where the putative Fe oxidizers may contribute significantly to the formation of these deposits. Furthermore, features of microbial communities inhabited in these deposits such as diversity, abundance and composition have not been fully illustrated (Al-Hanbali *et al.*, 2001; Peng *et al.*, 2007, 2010).

The Lau Basin is a back-arc spreading centre in the south-west Pacific. The Eastern Lau Spreading Center (ELSC), located within the basin from 19°20′S to 22°45′S, includes six known hydrothermal fields. According to previous studies, their deep lavas, vent fluid chemistry, mineralogy, geochemistry of hydrothermal deposits and microbial ecology vary considerably within the basin and are different from other well-studied hydrothermal vent sites in the Pacific Ocean (Reno, 2006; Hsu-Kim *et al.*, 2008). In this study, we present results of microbiological, geochemical and mineralogical analyses and discuss microbial diversity and abundance and the role microorganisms have played in mineral precipitation in the recently discovered 'CDE' hydrothermal field in ESLC (Zhou *et al.*, 2008).

Materials and methods

Study site and sample collection

The CDE hydrothermal field is located on the Eastern Lau Spreading Center (ELSC) at 176°11′W, 20°40′S. It was discovered by R/V DaYang YiHao (Ocean One) in May 2007 and is about four miles south of the ABE hydrothermal field (Fig. 1) (Zhou *et al.*, 2008). Chemosynthetic communities (anemones and crabs) and white microbial mats attached to pillar chimneys with heights from < 1 m to more than 5 m were found at the site using a deep tow camera system. Abnormity of turbidity (ΔNTU = 0.07), temperature (0.03 °C) and CH_4 (5.36 nM) were detected at the water column above the CDE hydrothermal field, by deep-water surveys using MAPR, CTD and onboard GC analysis of water samples, respectively. Low-temperature hydrothermal Fe–Si-rich precipitates were collected by a TV-grab (station No.19IV-TVG13) near hydrothermal chimneys at a depth of 2200 m. *In situ* temperatures of these precipitates were not measured because of the sampling technique limitations. Immediately after retrieval, samples were frozen and stored until further analyses.

Mineralogy and chemical analysis

Iron–silica-rich precipitates were dried at approximately 50 °C and thoroughly ground using a mortar and pestle.

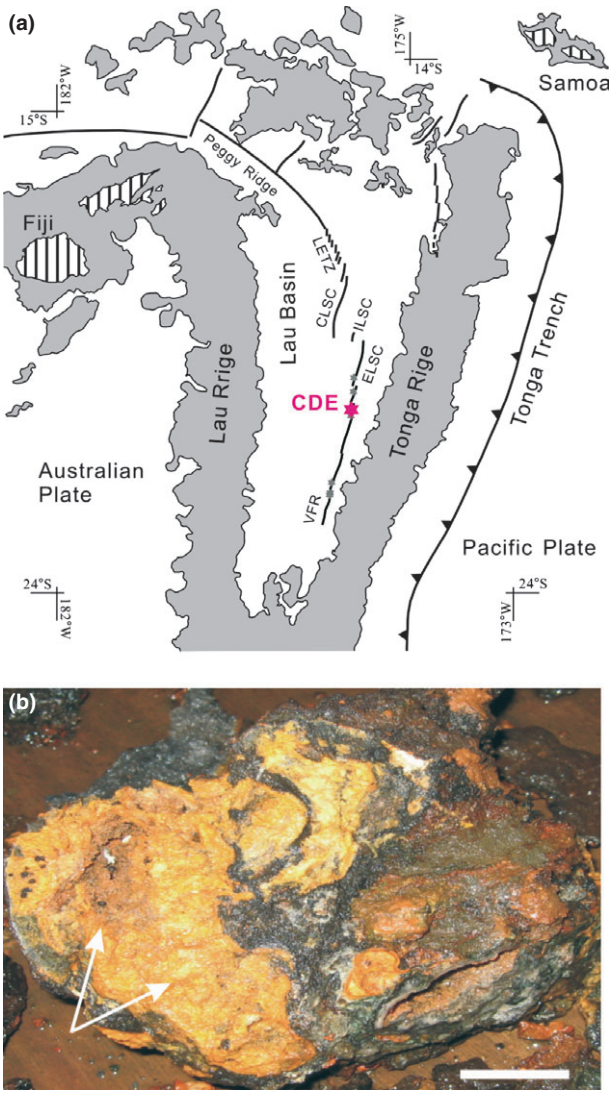

Fig. 1. Lau basin location diagrams and hydrothermal precipitates collected from CDE field. (a) Map of Lau basin with seven known hydrothermal field (labelled by star). CLSC-Central Lau Spreading Center; ILSC-Intermediate Lau Spreading Center; ELSC-East Lau Spreading Center; VFR-Valu Fa Ridge. (b) Low-temperature hydrothermal precipitates collected from new CDE hydrothermal field. Arrows indicate Fe-Si-rich precipitates (scale bar 5 cm).

X-ray diffraction (XRD) pattern analysis was then performed by a Rint 2000 X-ray diffractometer (Rigaku Corporation, Tokyo, Japan) using Cu Kα radiation at 40 kV and 30 mA. Diffraction angles (referred to as '2θ') corresponding to the atomic structure unique to each mineral were measured. Bulk chemical analyses were carried out using X-ray fluorescence (XRF) and ICP-MS at the Guangzhou Institute of Geochemistry, Chinese Academy of Sciences, China.

Morphological observation and ultrastructure analysis

Samples were examined using FEI Quant 400 environmental scanning electron microscopy (ESEM, the Netherlands). Gold coating on sample surfaces was not required for wet samples using environmental SEM, which avoided pretreatments on spectral analysis. In addition, we examined the ultrastructure of the hydrothermal precipitates with transmission electron microscopy (TEM). Small fragments fixed in 4% glutaraldehyde were prepared by washing three times with 0.1 M phosphate buffer (pH 7.4), further fixed with osmium tetroxide at 4 °C for 2 h and dehydrated through a series of ethanol solutions (10%, 20%, 30%, 40%, 50%, 60%, 70%, 80%, 90% and 100%, 10 min each). Dehydrated samples were then washed twice in propylene oxide, followed by overnight stand in a 50/50 mixture of propylene oxide and Agar100 resin. Samples were then allowed to stand in 100% resin for 24 h and then transferred into fresh embedding tubes where they were set in fresh resin and polymerized at 60 °C for 24 h. The samples were then sectioned on an ultramicrotome, mounted on copper grids and stained with uranyl acetate and lead citrate to improve contrast. Micro-area chemical composition of mineral surfaces was analysed on a Genesis energy dispersive spectrometer (EDAX).

DNA extraction, amplification and cloning

The DNA was extracted by SDS-based extraction with some modification (Zhou *et al.*, 1996). In brief, about 5 g of samples was mixed with 13.5 mL of DNA extraction buffer (100 mM Tris–HCl, 100 mM sodium EDTA, 100 mM sodium phosphate, 1.5 M NaCl, 1% CTAB) and 100 μL of proteinase K (10 mg mL^{-1}; Sigma) in tubes by horizontal shaking at 225 r.p.m. for 30 min at 37 °C. After shaking, 1.5 mL of 20% (w/v) SDS was added and samples were incubated in a 65 °C water bath for 2 h. The supernatants were collected after centrifugation at 6000 ***g*** for 10 min and transferred into 50-ml centrifuge tubes. The supernatants were mixed with an equal volume of chloroform isoamyl alcohol (24 : 1, v/v). The aqueous phase was recovered by centrifugation and precipitated with 0.6 volume of isopropanol for about 1 h. Crude nucleic acids were obtained by centrifugation at 16 000 ***g*** for 20 min at room temperature, washed with 70% ethanol and resuspended in sterile deionized water. The crude nucleic acids were purified with a cycle-pure kit (Omega).

The 16S rRNA genes were amplified by universal bacterial and archaeal primers (Lane, 1991; Delong, 1992). Bacterial 16S rRNA gene was amplified using Eubac27f (5′-AGA GTT TGA TCC TGG CTC AG-3′)/Eubac1492r (5′-GGT TAC CTT GTT ACG ACT T-3′); and Arch21f (5′-TTC CGG TTG ATC CYG CCG GA-3′)/Arch958r (5′-YCC GGC GTT GAM TCC AAT T-3′) were used for archaea with products of 1500 and 900 bp, respectively. Amplification conditions were as follows: an initial denaturalization step of 94 °C for 4min and then denaturation at 94 °C for 60 s, annealing at 55 °C for 45 s, and extension at 72 °C for 60 s for a total of 30 cycles, followed by a final extension of 72 °C for 10 min. All the PCR products were purified with a Gel-extraction kit (Omega) following the manufacturer's instructions. Purified PCR products were cloned into the pMD18-T vectors (Takara, Japan) and transformed to competent *Escherichia coli* DH5α cells (Takara). The PCR of the bacterial colonies was used to screen the presence of the correct-size inserts with the vector-specific primers M13f (5′-GTA AAA CGA CGG CCA G-3′) and M13r (5′-CAG GAA ACA GCT ATG AC-3′). Clones containing target 16S rRNA gene were subjected to restriction fragment length polymorphism (RFLP) analysis. Representative clones of archaea and bacteria with unique RFLP banding patterns were chosen for sequencing.

Quantification of 16S rRNA gene

Quantification of the microbial 16S rRNA gene was performed by fluorescence quantitative real-time PCR. Amplification was performed on the 7500 real-time PCR system (Applied Biosystems) in 20-μL reaction mixture, which consisted of 1 μL of template DNA (10 ng), a 0.15 μM concentration of each primer and 10 μL of Power SYBR green PCR master mix (Applied Biosystems) with ROX and SYBR green I. Melting curve analysis was performed after amplification, and the cycle threshold was set automatically using system 7500 software (1.3). Primers used to amplify the 16S rRNA gene were selected according to previous research (Treusch *et al.*, 2005; Nunoura & Takai, 2009).

Sequencing and phylogenetic analysis

Representative clones were directly sequenced by dideoxynucleotide chain termination using an ABI 3730 capillary electrophoresis sequencer (Applied Biosystems) with T-vector universal primers, M13f and M13r. The whole insert sequences were spliced by DNAMAN software (version 6.0), and the vector sequences were deleted. Archaeal and bacterial 16S rRNA gene sequences were obtained with lengths of about 900 and 1500 bp, respectively. Chimeric sequences were checked using BELLEROPHON (3.0) at www.greengenes.lbl.gov (Huber *et al.*, 2004; DeSantis *et al.*, 2006). The program DOTUR was used to determine the

operation taxonomic units (OTUs) for each sequence using a 97% similarity cut-off. Nonchimeric sequences were submitted to the Advanced BLAST search programme (available through the National Center for Biotechnology Information) to find closely related sequences in GenBank and EMBL databases for phylogenetic analysis. All clones sequences and matched sequences were aligned using the software CLUSTALX 1.83, and alignment positions with gaps were removed. Phylogenetic trees were constructed by neighbour-joining (NJ) using MEGA (5.05) with default parameters (Tamura *et al.*, 2011). Bootstrap analysis was used to provide confidence estimates of tree topologies.

Nucleotide sequence accession numbers

The sequences reported in this study were deposited in the GenBank database. Bacterial sequences have GenBank accession numbers GU220728–GU220769 and archaeal sequences GU207312–GU207319, respectively.

Results

Mineralogy and bulk chemistry

The Fe–Si-rich hydrothermal precipitates had a yellow interior with black to orange coatings. X-ray diffractometry (XRD) was used to identify different mineral phases. Results indicate that our samples were poorly crystallized. According to the XRD traces, the samples were composed mainly of amorphous silica, with a scattering broad band of maximum intensity centred at about 4 Å (22° 2θ), similar to opal-A (Rodgers *et al.*, 2004). The proportion of opal-A was > 90%, forming the dominant phase present in the precipitates. However, we did not detect any iron oxyhydroxides such as the two-line ferrihydrite and goethite.

Major chemical analysis by X-ray fluorescence (XRF) revealed that the hydrothermal deposits were rich in Si (74.2 wt%, SiO_2). Although no iron oxyhydroxides appeared according to XRD results, relatively high concentrations of Fe_2O_3 (about 9.8 wt%) were detected. Concentrations of other major elements (Al, Ca, K, Mg, Mn, Na, Sr, Cr, P) ranged from 0.1 to 1.3 wt% (Supporting Information, Table S1).

Morphological observation and description

The microscale morphologies of the hydrothermal precipitants were examined using environmental scanning electron microscopy (ESEM). Delicate structures such as filaments, stalks, rods, spheres and their aggregates were observed. Filament morphology was particularly variable and ranged from short simple-branching filaments to complex filament networks. Some were remarkably similar to bacterial-like structures.

Straight filaments

Straight filaments were abundant and frequently entwined with each other, with dense arrays throughout the precipitates (Fig. 2a–c). The filaments or long bacilliforms were tens to near a hundred micrometre long, with external diameters between 0.5 and 1.5 μm. Occasionally, irregular-shaped grains with diameters of 0.5–2.0 μm occurred on the surface of filaments (Fig. 2b). These rod-like structures resembled the sheath of *Leptothrix ochracea*, a well-known iron-oxidizing bacterium (FeOB). EDS analyses confirmed that the surfaces of these structures were mainly encrusted by amorphous silica (SiO_2). In addition, although the surfaces of these nonbranching silicified bacterial-like structures seemed smooth, many ringed grooves were observed after magnification (Fig. 2c,d). Uneven precipitation of amorphous silica may be responsible for the occurrence of these ringed grooves mentioned above.

Ribbon-like helical stalks

The distinctive filamentous ribbon-like helical stalks were recognized from the iron–silica precipitates (Fig. 2h). These special structures closely resembled those biogenic Fe-rich oxides produced by neutrophilic Fe-oxidizing bacteria such as *Gallionella ferruginea* and *Mariprofundus ferrooxydans*. EDS analysis showed that the distinctive filamentous ribbon-like helical stalk was mainly composed of Si (28.77 wt%), Fe (21.22 wt%) and O (48.76 wt%). The unique features of these stalks included the ribbon-like regular helical or twisted morphologies generally present in iron-rich microbial mats from deep-sea hydrothermal fields or subterranean environments (Ferris *et al.*, 1999; Emerson & Moyer, 2002; Edwards *et al.*, 2004). As products of FeOBs metabolic activity, their occurrences were used as direct evidence of bacteriogenic mineralization (Chan *et al.*, 2011).

Curved filaments and branching filaments

Commonly occurring, curved filamentous structures were also observed (Fig. 2f,g). These structures varied from several to tens micrometre, occasionally up to a 100 μm in length. Some were also bifurcated and formed branching filaments (Fig. 2g). Based on the observed morphologies, the curved filaments and stalk-like fragments resembled the extracellular filamentous material produced by *M. ferrooxydans* PV-1 strain (Emerson & Moyer, 2002; Emerson *et al.*, 2007). SEM–EDS analyses indicated that

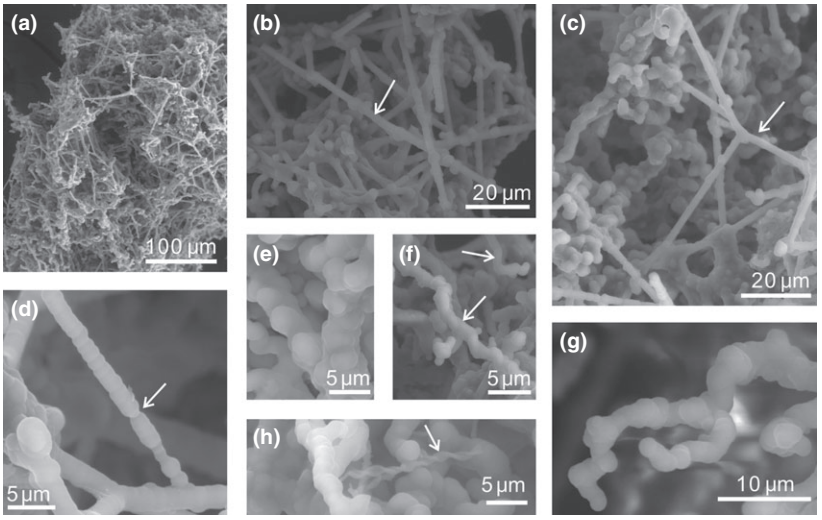

Fig. 2. SEM images of hydrothermal precipitates, exhibiting special and delicate morphologies. (a) aggregates of straight filamentous structures; (b,c) silicification of filamentous microbe-like structures, which formed typical straight filaments (arrow). EDS indicates that they were heavily coated by amorphous silicon (opal-A); (d) As pointed by arrow, ringed grooves were obvious at higher magnification; (e) the oblate or imperfect opal-A microspheres developed on the surfaces of filaments; (f,g) curved, nonhelical structures (pointed by arrows) resembling the filaments of *Mariprofundus ferrooxydans* strain PV-1 (Emerson & Moyer, 2002); (h) helical ribbon-like morphologies (arrow) resembling the stalk of *Gallionella ferruginea* and *M. ferrooxydans*.

all these filaments appeared to be heavily encrusted with siliceous precipitates (SiO_2).

Globular aggregates

In addition to those distinctive morphologies described above, colloid particles with irregular spherical shapes were also abundant and dominated the analysed deposits (Fig. 2e). Usually, they agglomerated upon suitable substrates and formed globular aggregates with diameters varying from 0.5 to 20 μm. Occasionally, these microspheres coagulated and became loosely interwoven, which helped cement various microbe-like structures. Chemical analyses indicated that these aggregates were composed of a gel-like material rich in SiO_2. From morphologies, composition and mineralogy, we conclude that these structures were likely the first-phase silica deposits, that is, opal-A (Rodgers *et al.*, 2004).

Transmission electron microscopy

Examination of the samples by TEM and EDS revealed two different types of mineralization. The first type was silicification, mainly related to siliceous precipitation (Fig. 3b,c), while the second was chiefly involved in the formation of iron oxyhydroxide (Fig. 3a). Amorphous siliceous precipitation was common and often formed various spheres, irregular morphologies and their aggregates (as shown in Fig. 3b). The cross-sections of some filaments exhibited hollow structures with relatively rough walls. Noticeably, the walls of different hollow structures had different chemical components, which were mainly composed of either silica (Fig. 3c) or iron oxyhydroxide (Fig. 3a). Cross-sections showed that some filaments were filled with an iron-rich matrix surrounded by amorphous silica (Fig. 3e). TEM revealed a linear chain of Fe-rich oxyhydroxides in the centre of the filaments encrusted by a siliceous matrix (Fig. 3f,g). In addition, TEM observations of thin cross-sections found that some cells were undergoing intracellular mineralization, with the cytoplasm being replaced by amorphous materials in the lysed bacterial cells (Fig. 3d). Energy dispersive X-ray spectroscopy indicated that the cell walls had higher iron and silicon content (18.61 and 3.93 wt%) than the inner materials (3.72 and 1.37 wt%, respectively). TEM–EDS analysis suggested that microbe-like structures were generally encrusted by amorphous silica, indicating their role as nucleation site for the silica precipitation.

Quantitative PCR of the small subunit (SSU) 16S rRNA gene and biomass estimation

The results of the qPCR indicated that the number of archaeal 16S rRNA genes were about 6.21×10^7 copies per gram of hydrothermal precipitates, while the bacterial 16S rRNA genes were about 1.22×10^8 copies per gram. Based on the qPCR results and assuming an average 16S rRNA gene copy number of 4.17 and 1.71 per cell for

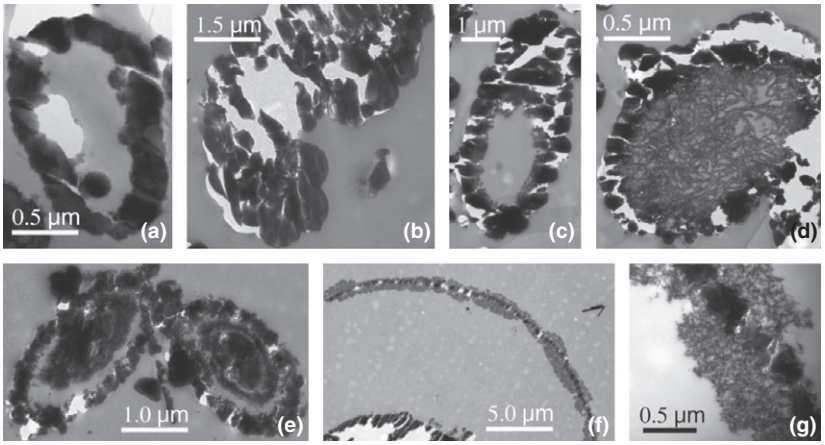

Fig. 3. TEM images of iron–silica-rich hydrothermal precipitates. (a) The cross-section of a filament exhibiting a hollow structure. The wall consists of iron-rich matrix (11.99 wt%) with 2.60 wt% of silica. (b) Aggregates of siliceous precipitates, which are mainly composed of amorphous silica. (c) A cross-section of the filamentous structures. The inner iron-rich parts are coated by the siliceous outer walls. (d) Cell undergoing intracellular mineralization with the cytoplasm being replaced by amorphous materials. (e) iron-rich matrix surrounded by amorphous silica. (f,g) The filamentous structure with a Fe-rich core encrusted heavily by amorphous silica.

bacteria and archaea (Lee *et al.*, 2009), we estimated that the cell densities of bacteria and archaea inhabited in our precipitates were 2.93×10^7 and 3.63×10^7 cells g^{-1}, respectively.

Diversity of 16S rRNA genes

Phylogenetic analyses of PCR-amplified 16S rRNA gene from the hydrothermal precipitates were carried out to investigate the microbial communities in the precipitates.

Archaeal SSU rRNA gene clone analysis

Eight unique archaeal 16S rRNA gene phylotypes were identified from a total of 76 representative clones. Five of the phylotypes (including 68 clones) were primarily affiliated with the marine group I (MGI) Crenarchaeota group. Members of this group are almost ubiquitous in various oceanic environments, and sequences related to our phylotypes have been detected mainly in deep-sea sediments on the Pacific Nodule Province, Japan Trench, Nankai Trough, and the Antarctic and Aegean Seas (Fig. 4). Noticeably, sequences similar to phylotype TVG13-A8 and A66 included the only pure culture of MGI, *Nitrosopumilus maritimus* (identity = 97–98%), an autotrophic ammonia-oxidizing marine archaea that grows chemolithoautotrophically by aerobically oxidizing ammonia to nitrite (Konneke *et al.*, 2005). In the present study, 25 clones were closely related to phylotypes TVG13-A8 and A66, accounting for 33% of the archaeal library. In addition, three residual phylotypes (representing eight clones) were of archaeal lineage and classified as Euryarchaeota (Fig. 4 and Table S2).

Bacterial SSU rRNA gene clone analysis

A total of 78 positive clones from the bacterial 16S library were analysed, with 41 phylotypes identified for phylogenetic analysis. These sequences mainly fell within Proteobacteria (α-, β-, γ-, δ-, ε- and ζ-), Verrucomicrobia and Planctomycetes (Fig. 5, Fig. S1 and Table S3).

Members of α-Proteobacteria contained 20 phylotypes (representing 36 clones) and dominated the bacterial communities, accounting for 46% of the total clones. Within α-Proteobacteria, bacterial populations were diverse and covered various subclasses such as Rhizobiales, Rhodobacterales, Kordiimonadales and Rhodospirillales (Fig. S1). Five phylotypes (seven clones) were assigned to Rhizobiales and were most closely related to sequences from uncultivated organisms in various sea floor hydrothermal environments, such as sediments, lavas and submarine hot spring. Bacteria belonging to Rhodospirillales included three phylotypes representing three clones. Together with several pure cultures, this phylogenetic clade was formed from the clones and environmental sequences of the Pacific Ocean, Sargasso Sea, eastern Mediterranean Sea, Loi′hi Seamount and Antarctic Booney. Sequences affiliated to Rhodobacterales and Kordiimonadales constituted 17% (four phylotypes, nine clones) and 4% (one phylotype, four clones) of the bacterial sequences, respectively. Other sequences within α-Proteobacteria showed high similarity to uncultivated organisms and low similarity to cultured species (generally < 91%).

Six phylotypes, including 13 clones with a proportion of 16.7%, were identical to the members of ε-Proteobacteria. Most of the phylotypes were related to clones or isolates from different marine environments such as

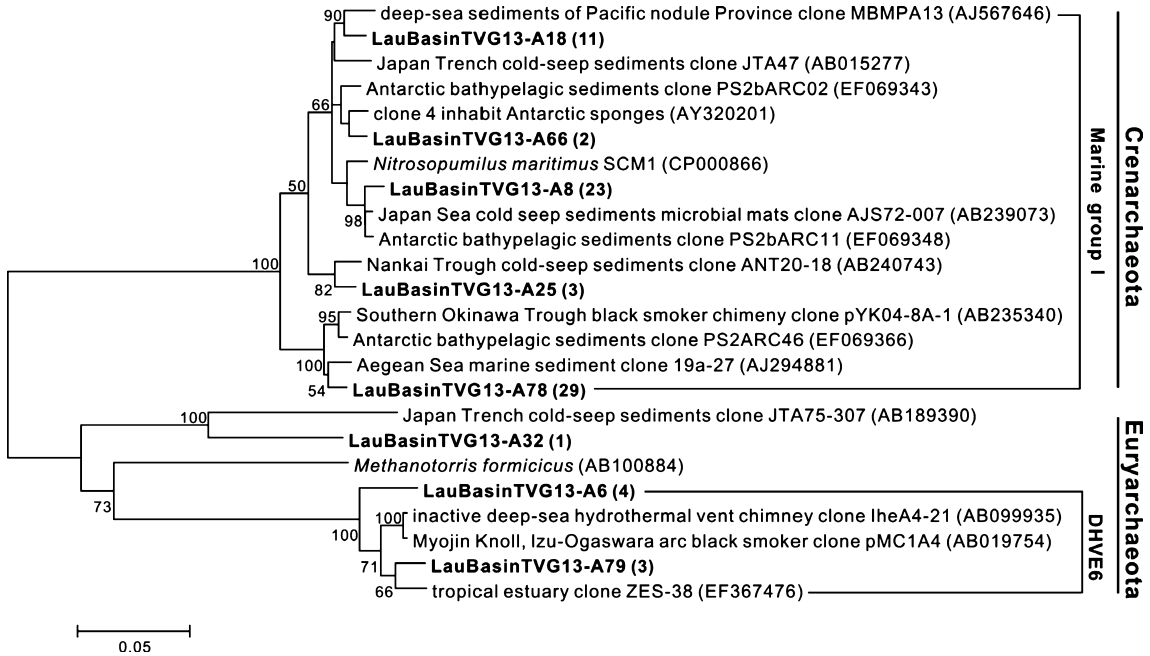

Fig. 4. Phylogenetic relationships of representative archaea clones obtained from CDE hydrothermal field of Lau Basin. The tree was constructed by neighbour-joining analysis of 16S rRNA gene sequences with software MEGA 5.05. Clones from this study were denoted in bold-type face. The numbers in parentheses are the GenBank accession numbers for sequences obtained from NCBI except for our clones. Bootstrap percentages are obtained using 1000 replicates, and values > 50% are indicated at the nodes. The scale bar represents the expected number of changes per nucleotide position.

hydrothermal chimney, cold-seep and sediments (Fig. 5). The distributions of other groups were as follows: β-Proteobacteria (one phylotype, one clones), γ-Proteobacteria (three phylotypes, five clones), δ-Proteobacteria (four phylotypes, eight clones), candidate ζ-Proteobacteria (two phylotypes, eight clones), Verrucomicrobia (one phylotype, two clones) and Planctomycetes (three phylotypes, four clones). In addition, one phylotypes (TVG13-B7) branched into unclassified groups owing to their low similarity to known sequences.

Notably, several phylotypes aligned well with those well-known Fe-oxidizing bacteria. Phylotype TVG13-B96 (representing one clone) fell into β-Proteobacteria and shared highest (97%) sequence similarity with the *Gallionella* phylotype YS18Uc25 obtained from Fe–Si-rich microbial mats at the hydrothermal field of the Southern Mariana Trough (Kato *et al.*, 2009). We also detected another important group involved in Fe-oxidation, specifically, a new *Candidatus* class of Proteobacteria (ζ-proteobacteria) widely distributed in deep-sea environments (Emerson *et al.*, 2007). Two phylotypes, TVG13-B2 and B40, were aligned with the cultivated iron-oxidizing organism *M. ferrooxydans* and environmental clones within this group obtained from various hydrothermal vents systems.

Discussion

The dominance of amorphous opal-A and low concentrations of metals suggest that Fe–Si-rich precipitates studied in this paper belong to typical low-temperature hydrothermal deposits, which were probably precipitated from low-temperature hydrothermal fluids (Boyd & Scott, 2001). Although some abiological processes could result in microorganism-like micro-textures (Garcia-Ruiz, 1998), morphological characteristics observed in our samples afford further support of their bacteriogenic origin. Typical morphologies observed in our study include filamentous and stalk-like forms. These filamentous structures were abundant and geometrically consistent with the size, form and aggregation of microorganisms, suggesting that microorganisms probably have played an important role in the mineralization.

Biomineralization related to neutrophilic iron oxidizers

Tubular sheaths, helical or twisted stalks and slender or irregular filaments, which are characteristic and distinguishable biosignatures, are generally considered as reliable indicators of biomineralization involving the FeOBs

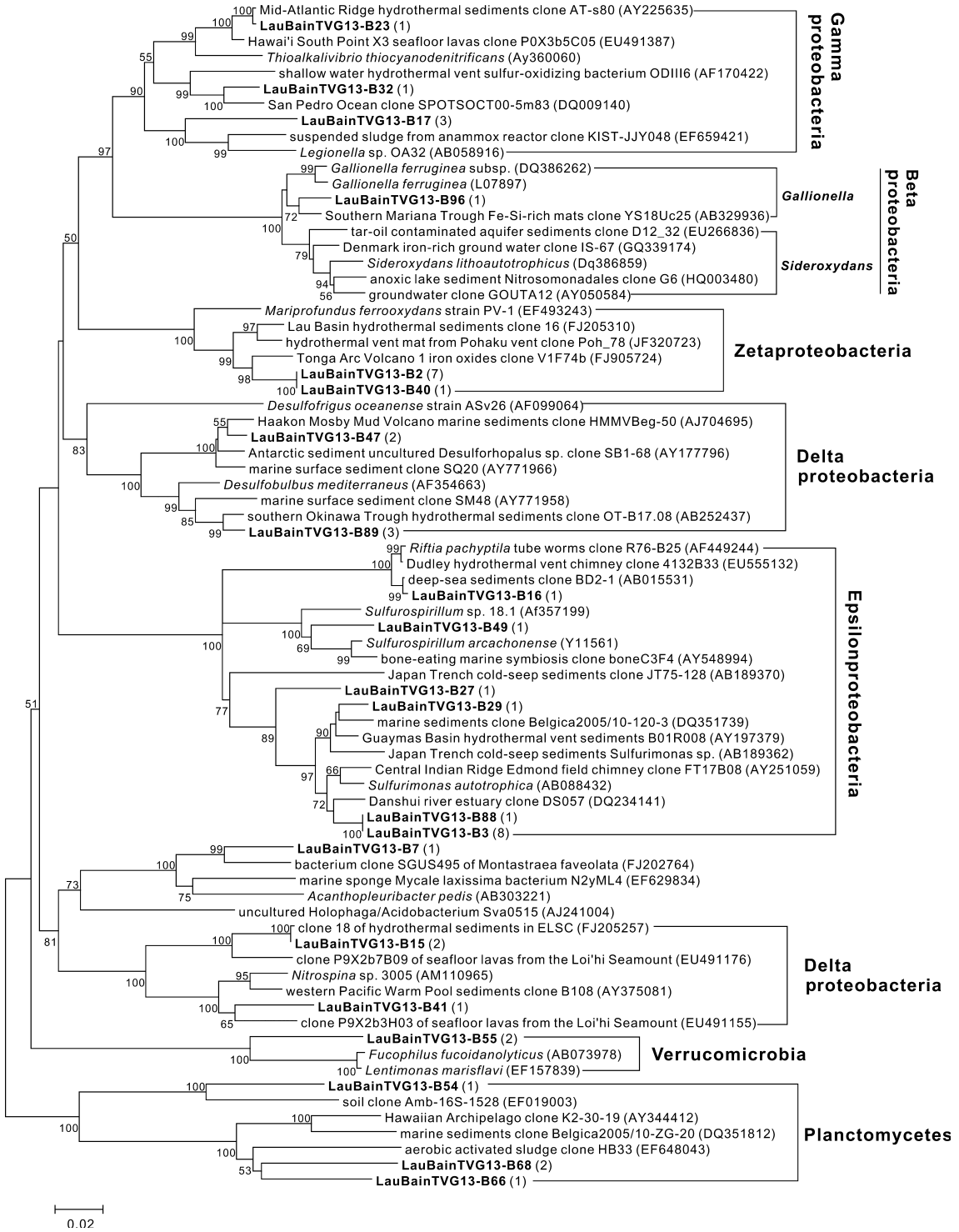

Fig. 5. Phylogenetic relationship of bacterial 16S rRNA gene sequences except for α-Proteobacteria obtained from Lau Basin. The tree was inferred by neighbour-joining analysis with software MEGA 5.05. Clones from this study were denoted in bold-type face. The numbers in parentheses are the GenBank accession numbers for sequences obtained from NCBI except for our clones. Bootstrap percentages are obtained using 1000 replicates, and values > 50% are indicated at the nodes. The scale bar represents the expected number of changes per nucleotide position.

(Juniper & Fouquet, 1988; Emerson & Moyer, 2002; Emerson *et al.*, 2007; Chan *et al.*, 2011). Previous studies have established the corresponding relationship between those distinctive morphologies and certain species of the known FeOBs (Emerson & Moyer, 2002; Emerson *et al.*, 2010; McAllister *et al.*, 2011). In this study, the samples contained numerous filamentous structures whose morphologies were similar to those produced by known FeOBs. Among these characteristic structures, helical stalks shown in Fig. 2 are the most commonly observed structures, offering supporting evidence for a biological origin of these structures, which were likely formed by *G. ferruginea* or *M. ferrooxydans.* Generally, these FeOBs obtain energy from Fe-oxidation ($Fe^{2+} \rightarrow Fe^{3+}$) and form Fe-rich stalks to eliminate the ferric waste product (Chan *et al.*, 2011; Suzuki *et al.*, 2011). Emerson *et al.* (2007) demonstrated that iron-oxidizing bacteria *M. ferrooxydans* produced filamentous stalk-like structures composed of Fe oxyhydroxide during chemolithotrophic growth. Our SEM–EDS results showed that the stalk-like microstructures in our samples were mainly composed of iron-rich materials. Phylogenetic analyses confirm the presence of the FeOBs known for their direct involvement in the formation of Fe-rich precipitates. The two phylotypes (TVG13-B2, B40) detected in the precipitates aligned well with *M. ferrooxydans* and other sequences within the ζ-proteobacteria group (Fig. 5). One phylotype, TVG13-B96, showed high identity to *Gallionella.* spp. Thus, on the basis of ultrastructural and phylogenetic analyses, we tentatively conclude that the tubular sheaths, filaments, helical and twisted stalks observed in the CDE hydrothermal field are of bacteriogenic origin, formed probably with the involvement of FeOBs.

Interestingly, we detected one clone related to *Gallionella* in the β-proteobacteria class. Phylotype TVG13-B96 showed high identity (97%) to clone YS18Uc25, which is the only *Gallionella* phylotype detected from deep-sea hydrothermal environments (Kato *et al.*, 2009). As discussed in early reports (e.g. Kennedy *et al.*, 2003), it was initially assumed that ribbon-like helical stalks were produced by freshwater *Gallionella* spp., almost no sequence data or convincing microbial evidence exist to confirm the occurrence of *Gallionella* in marine environments. With the isolation of *M. ferrooxydans* (Emerson & Moyer, 2002; Emerson *et al.*, 2007), which could produce strikingly similar Fe-rich stalks but is phylogenetically distant from *Gallionella*, it was proposed that those stalks should be ascribed to ζ-proteobacteria because it has been widely detected in diverse hydrothermal habitats around the world. Together with YS18Uc25, our results suggest that members related to *Gallionella* indeed exist in deep-sea hydrothermal vents and probably contribute to biomineralization of iron.

The role of microorganisms in silicification

Results of morphological observation and chemical analysis indicate that silicification was a common mineralizing phenomenon in our CDE hydrothermal precipitates. SEM- and TEM–EDS analyses showed that many microstructures were heavily encrusted by amorphous silica and those siliceous spherules, strumae and irregular forms could aggregate on the surfaces of structures (Figs 2 and 3). Although the role of microorganisms in mediating silicification remains debated, it has been suggested that microbial cell surfaces and their extracellular polymers can act as excellent nucleation sites for silica precipitation (Urrutia & Beveridge, 1993; Fein *et al.*, 2002; Phoenix *et al.*, 2003; Konhauser *et al.*, 2004). When hydrothermal fluids with high concentrations of dissolved silica are mixed with ambient low-temperature fluids, amorphous silica rapidly precipitates on the surface of multifarious materials for the reduced solubility and then forms amorphous opal-A. Once the encrusted core (microbial cell or their organic affiliates) decomposes, the siliceous crusts would remain and cause the observed central hollow canals as shown in Fig. 3c.

Biogenic ultrastructures related to FeOBs, including stalks and various filaments, probably also served as the scaffolding for silica accumulation and precipitation and thus contributed significantly to silicification in our samples. Simulation experiments suggest that Fe plays an important role in the precipitation of silica (Fein *et al.*, 2002) and can significantly accelerate the rate and extent of Si removal from solutions (Yee *et al.*, 2003). Therefore, filamentous structures typically are heavily encrusted by amorphous silica (Fig. 2). Among the TEM micrographs, we observed an iron-rich filamentous core surrounded by a matrix of silica (Fig. 3f,g). Even the fresh-looking ribbon-like helical stalk was also coated by the SiO_2 (Fig. 2h), suggesting that biogenic filamentous structure may have served as templates for silica precipitation.

Microbial diversity inhabited in the Fe–Si-rich precipitates of the CDE Field

Up to date, numerous molecular analyses have been carried out to investigate bacterial communities related to low-temperature hydrothermal Fe–Si-rich precipitates (Emerson & Moyer, 2002; Davis *et al.*, 2009; Hodges & Olson, 2009; Kato *et al.*, 2009; Rassa *et al.*, 2009; Forget *et al.*, 2010; Edwards *et al.*, 2011; McAllister *et al.*, 2011). Most of the studies showed that ζ-proteobacteria, including the only isolate *M. ferrooxydans* and related uncultured clones, are abundant and predominant. However, our molecular analysis revealed obviously different and diverse bacterial communities. A variety of bacterial 16S

rRNA gene phylotypes were recovered from the Fe–Si-rich precipitate samples. Members of α-proteobacteria instead of FeOBs-related groups dominated the bacterial clone library (46.0% of the clone library). Although α-proteobacteria are widely distributed in various marine environments such as surface seawater, water column, sediments and hydrothermal environments, sequences closely related to our phylotypes mainly come from sediments (as shown in Table S3). The ε-proteobacteria were the next largest group accounting for 16.7% of the clone library. Phylotypes within this group were closely related to the known *Sulphurimonas* spp. and *Sulphurospirillum* spp. (Fig. 5), which are sulphur cycle-related bacteria (Inagaki *et al.*, 2003). In addition, members of γ- and δ-proteobacteria also occurred with low proportions. Members of the known FeOBs such as *Gallinella* and ζ-proteobacteria were relatively low in abundance. Generally, the abundance of FeOBs is closely related to the concentrations of ferrous iron in the hydrothermal fluids and the low abundance of FeOBs means that the supply of Fe^{2+} was probably limited. So most of biosignatures detected in this study probably are the remnants of earlier activities of FeOBs. With the decreasing ferric iron concentrations, the majority of FeOBs probably died off and disappeared.

In contrast to the extensive eubacteria investigations, archaeal community composition has been rarely reported in such environments (Moyer *et al.*, 1995; Kato *et al.*, 2009). Representatives of the MGI were the largest group and dominated in the archaeal library (accounting for 90%) in our samples. Moreover, nearly 33% of the clones within MGI showed high sequence similarity (97–98%) to *N. maritimus*, a chemolithoautotrophic ammonia oxidizer (Konneke *et al.*, 2005). This strongly suggests that ammonia oxidation was common and the related microorganisms likely contributed to the carbon and nitrogen cycle in the CDE hydrothermal field. Data from the *amoA* functional gene analysis also supported this conclusion (data not shown). In addition, phylotypes fallen into the DHVE group were also detected (TVG13-A6 and TVG13-A79, representing seven clones). As the DHVE group are generally considered to be restricted to high-temperature hydrothermal environments (Hoek *et al.*, 2003; Reysenbach *et al.*, 2006), the detection of the DHVE groups in low-temperature hydrothermal niches implies that these phylotypes probably come from the vicinal high-temperature vents.

Conclusions

In conclusion, this study revealed the occurrence of microbial mineralization and microbial communities in the low-temperature hydrothermal precipitates of the CDE field located at ESLC. We described distinct ultrastructures produced by unique microorganisms and characterized biomineralization involving the FeOBs and silicification. Special morphological characteristics are good indicators for recognizing biological signatures in modern and fossil hydrothermal vent environments. Although morphological characteristics are similar to what was observed in other hydrothermal environments, microbial diversity, abundance and component inhabited in these precipitates are distinctive. However, because of the limitations in our sampling procedures, the lack of basic environmental parameters hinders our interpretation for the possible reasons of the differences. It is important to note that our samples, mainly composed of amorphous silica (SiO_2, 74.2 wt%) with much less iron (Fe_2O_3, 9.8 wt%) are obviously different from those Fe-rich flocculent mats consisting dominantly of iron oxides/oxyhydroxides with variable amounts of silica. The difference in mineralogy and chemical composition indicates the different venting fluid characteristics and precipitating stage (Halbach *et al.*, 2002), which could have significantly influenced the microbial composition in our Fe–Si-rich precipitates present here. Nevertheless, the present study provides valuable insights into microbial mineralization and microbiology of Fe–Si-rich precipitates in deep-sea low-temperature hydrothermal environments.

Acknowledgements

We are grateful to Christian Griebler and two anonymous reviewers whose insightful comments and suggestions greatly improved the manuscript. We thank all crew members of R/V DaYang YiHao for retrieving the samples studied. The authors would like to warmly thank Dr David Emerson for information regarding iron-oxidizing bacteria. This work was financially supported by the National Natural Science Foundation of China (NSFC, No. 41002122) and National Basic Research Program of China (973 Program, No. 2012CB417300).

References

Al-Hanbali HS, Sowerby SJ & Holm NG (2001) Biogenicity of silicified microbes from a hydrothermal system: relevance to the search for evidence of life on earth and other planets. *Earth Planet Sci Lett* **191**: 213–218.

Alt JC (1988) Hydrothermal oxide and nontronite deposits on seamounts in the Eastern Pacific. *Mar Geol* **81**: 227–239.

Boyd TD & Scott SD (2001) Microbial and hydrothermal aspects of ferric oxyhydroxides and ferrosic hydroxides: the example of Franklin Seamount, Western Woodlark Basin, Papua New Guinea. *Geochem Trans* **2**: 45.

Chan CS, Fakra SC, Emerson D *et al.* (2011) Lithotrophic iron-oxidizing bacteria produce organic stalks to control mineral growth: implication for biosignature formation. *ISME J* **5**: 717–727.

Davis RE, Stakes DS, Wheat CG *et al.* (2009) Bacterial variability within an iron-silica-manganese-rich hydrothermal mound located off-axis at the Cleft Segment, Juan de Fuca Ridge. *Geomicrobiol J* **26**: 570–580.

Delong EF (1992) Archaea in coastal marine environments. *Proc. Natl. Acad. Sci.* **89**: 5685–5689.

DeSantis TZ, Hugenholtz P, Keller K *et al.* (2006) NAST: a multiple sequence alignment server for comparative analysis of 16S rRNA genes. *Nucleic Acids Res* **34**: W394–W399.

Edwards KJ, Bach W, McCollom TM *et al.* (2004) Neutrophilic iron-oxidizing bacteria in the ocean: habitats, diversity, and roles in mineral deposition, rock alteration, and biomass production in the deep-sea. *Geomicrobiol J* **21**: 393–404.

Edwards KJ, Glazer BT, Rouxel OJ *et al.* (2011) Ultra-diffuse hydrothermal venting supports Fe-oxidizing bacteria and massive number deposition at 5000 m off Hawaii. *ISME J* **5**: 1748–1758.

Emerson D & Moyer CL (2002) Neutrophilic Fe-oxidizing bacteria are abundant at the Loihi Seamount hydrothermal vents and play a major role in Fe oxide deposition. *Appl Environ Microbiol* **68**: 3085–3093.

Emerson D, Rentz JA, Liburn TG, Davis RE, Aldrich H, Chan C & Moyer CL (2007) A novel lineage of Proteobacteria involved in formation of marine Fe-oxidizing microbial mat communities. *PLoS ONE* **8**: 1–9.

Emerson D, Fleming EJ & McBeth JM (2010) Iron-oxidizing bacteria: an environmental and genomic perspective. *Annu Rev Microbiol* **64**: 561–583.

Fein JB, Scott S & Rivera N (2002) The effect of Fe on Si adsorption by *Bacillus subtilis* cell walls: insights into non-metabolic bacterial precipitation of silicate minerals. *Chem Geol* **182**: 265–273.

Ferris FG, Konhauser KO, Lyven B *et al.* (1999) Accumulation of metals by bacteriogenic iron oxides in a subterranean environment. *Geomicrobiol J* **16**: 181–192.

Forget NL, Murdock SA & Juniper SK (2010) Bacterial diversity in Fe-rich hydrothermal sediments at two South Tonga Arc submarine volcanoes. *Geobiology* **8**: 417–432.

Fortin D, Ferris FG & Scott SD (1998) Formation of iron-silicates and iron oxides on bacterial surfaces in samples collected near hydrothermal vents on the Southern Explorer Ridge in the northeast Pacific Ocean. *Am Mineral* **83**: 1399–1408.

Garcia-Ruiz JM (1998) Carbonate precipitation in silica-rich environments. *Geology* **26**: 843–846.

Halbach M, Halbach P & Luders V (2002) Sulfide-impregnated and pure silica precipitates of hydrothermal origin from the Central Indian Ocean. *Chem Geol* **182**: 357–375.

Hodges TW & Olson JB (2009) Molecular comparison of bacterial communities within iron-containing flocculent mats associated with submarine volcanoes along the Kermadec Arc. *Appl Environ Microbiol* **75**: 1650–1657.

Hoek J, Banta A, Hubler F & Reysenbach A-L (2003) Microbial diversity of a sulphide spire located in the Edmond deep-sea hydrothermal vent filed on the Central Indian Ridge. *Geobiology* **1**: 119–127.

Hrischeva E & Scott SD (2007) Geochemistry and morphology of metalliferous sediments and oxyhydroxides from the Endeavour segment, Juan de Fuca Ridge. *Geochem Cosmochim Acta* **71**: 3476–3497.

Hsu-Kim H, Mullaugh KM, Tsang JJ, Yucel M & Luther GW III (2008) Formation of Zn- and Fe-sulfides near hydrothermal vents at he Eastern Lau Spreading Center: implications for sulfide bioavailability to chemoautotrophs. *Geochem Trans* **9**: 1–14.

Huber T, Faulkner G & Hugenholtz P (2004) Bellerophon: a program to detect chimeric sequences in multiple sequence alignments. *Bioinformatics* **20**: 2317–2319.

Inagaki F, Takai K, Kobayashi H, Nealson KH & Horikoshi K (2003) *Sulfurimonas autotrophica* gen. nov., sp. nov., a novel sulfur-oxidizing epsilon-proteobacterium isolated from hydrothermal sediments in the mid-Okinawa Trough. *Int J Syst Evol Microbiol* **53**: 1801–1805.

Juniper SK & Fouquet Y (1988) Filamentous iron-silica deposits from modern and ancient hydrothermal sites. *Can Mineral* **26**: 859–869.

Kato S, Kobayashi C, Kakegawa T & Yamagishi A (2009) Microbial communities in iron-silica-rich microbial mats at deep-sea hydrothermal fields of the southern Mariana Trough. *Environ Microbiol* **11**: 2094–2111.

Kennedy CB, Scott SD & Ferris FG (2003) Characterization of bacteriogenic iron oxide deposits from Axial Volcano, Juan de Fuca Ridge, northeast Pacific Ocean. *Geomicrobiol J* **20**: 199–214.

Konhauser KO, Jones B, Phoenix VR, Ferris G & Renaut RW (2004) The microbial role in hot spring silicification. *Ambio* **33**: 552–557.

Konneke M, Bernhard AE, de la Torre JR, Walker CB, Waterbury JB & Stahl DA (2005) Isolation of an autotrophic ammonia-oxidizing marine archaeon. *Nature* **437**: 543–546.

Lane DJ (1991) 16S/23S rRNA sequencing. Nucleic acid techniques in bacterial systematics (Stackebrandt E & Goodfellow M eds), p. 115–175. Wiley, Chichester, UK.

Langley S, Igric P, Takahashi Y *et al.* (2009) Preliminary characterization and biological reduction of putative biogenic iron oxides (BIOS) from the Tonga-Kermadec Arc, southwest Pacific Ocean. *Geobiology* **7**: 35–49.

Lee ZM, Bussema C III & Schmidt TM (2009) rrnDB: documenting the number of rRNA and tRNA genes in bacteria and archaea. *Nucleic Acids Res* **37**: D489–D493.

McAllister SM, Davis RE, McBeth JM *et al.* (2011) Biodiversity and emerging biogeography of the neutrophilic iron-oxidizing zetaproteobacteria. *Appl Environ Microbiol* **77**: 5445–5457.

Moyer CL, Dobbs FC & Karl DM (1995) Phylogenetic diversity of the bacterial community from a microbial mat at an active, hydrothermal vent system, Loihi Seamount, Hawaii. *Appl Environ Microbiol* **61**: 1555–1562.

Nunoura T & Takai K (2009) Comparison of microbial communities associated with phase-seperation-induced hydrothermal fluids at the Yonaguni Knoll IV hydrothermal field, the Southern Okinawa Trough. *FEMS Microbiol Ecol* **67**: 351–370.

Peng X, Zhou H, Yao H *et al.* (2007) Microbe-related precipitation of iron and silica in the Edmond deep-sea hydrothermal vent field on the Central Indian Ridge. *Chin Sci Bull* **52**: 3233–3238.

Peng X, Zhou H, Li J *et al.* (2010) Intracellular and extracellular mineralization of a microbial community in the Edmond deep-sea vent field environment. *Sed Geol* **229**: 193–206.

Peng X, Chen S, Zhou H *et al.* (2011) Diversity of biogenic minerals in low temperature Si-rich deposits from a newly discovered hydrothermal field on the ultra-slow spreading Southwest Indian Ridge. *J Geophys Res* **116**: G03030.

Phoenix VR, Konhauser KO & Ferris FG (2003) Experimental study of iron and silica immobilization by bacteria in mixed Fe-Si systems: implications for microbial silicification in hot springs. *Can J Earth Sci* **40**: 1669–1678.

Rassa AC, McAllister SM, Safran SA *et al.* (2009) Zeta-proteobacteria dominate the colonization and formation of microbial mats in low-temperature hydrothermal vents at Loihi Seamount, Hawaii. *Geomicrobiol J* **26**: 623–638.

Reno NV (2006) Ridge 2000 Workshop Report: Lau Integrated Studies Site Focus Workshop.

Reysenbach A-L, Liu YT, Banta AB & Beveridge TJ (2006) Isolation of a ubiquitous obligate thermoacidophilic archaeon from deep-sea hydrothermal vents. *Nature* **442**: 444–447.

Rodgers KA, Browneb PRL, Buddleb TF *et al.* (2004) Silica phases in sinters and residues from geothermal fields of New Zealand. *Earth Sci Rev* **66**: 1–61.

Suzuki T, Hashimoto H, Matsumoto N *et al.* (2011) Nanometer-scale visualization and structural analysis of the inorganic/organic hybrid structure of *Gallionella ferruginea* twisted stalks. *Appl Environ Microbiol* **77**: 2877–2881.

Tamura K, Peterson D, Peterson N *et al.* (2011) MEGA5: molecular evolutionary genetics analysis using maximum likelihood, evolutionary distance, and maximum parsimony methods. *Mol Biol Evol* **28**: 2731–2739.

Templeton AS, Knowles EJ, Eldridge DL *et al.* (2009) A seafloor microbial biome hosted within incipient ferromanganese crusts. *Nat Geosci* **2**: 872–876.

Treusch AH, Leininger S, Kletzin A, Schuster SC, Klenk HP & Schleper C (2005) Novel genes for nitrite reductase and Amo-related proteins indicate a role of uncultivated mesophilic Crenarchaeota in nitrogen cycling. *Environ Microbiol* **7**: 1985–1995.

Urrutia MM & Beveridge TJ (1993) Mechanism of silicate binding to the bacterial cell wall in *Bacillus subtilis*. *J Bacteriol* **175**: 1936–1945.

Yee N, Phoenix VR, Konhauser KO *et al.* (2003) The effects of cyanobacteria on silica precipitation at neutral pH: implication for bacterial silicification in geothermal hot springs. *Chem Geol* **199**: 83–90.

Zhou J, Bruns M & Tiedje J (1996) DNA recovery from soils of diverse composition. *Appl Environ Microbiol* **62**: 316–322.

Zhou HY, Li JT & Yang QH (2008) Microbiological oxidation of sulfide chimney promoted by warm diffusing flow in CDE hydrothermal field in Eastern Lau Spreading Center. AGU fall meeting.

Supporting Information

Additional Supporting Information may be found in the online version of this article:

Fig. S1. Phylogenetic relationship of α-Proteobacteria 16S rRNA gene sequences.
Table S1. Chemical compositions of the yellow hydrothermal precipitates revealed by the bulk chemical analysis.
Table S2. Summary of archaeal 16S rRNA gene clone sequences from Fe–Si-rich hydrothermal precipitates.
Table S3. Summary of bacterial 16S rRNA gene clone sequences from Fe–Si-rich hydrothermal precipitates.

Please note: Wiley-Blackwell is not responsible for the content or functionality of any supporting materials supplied by the authors. Any queries (other than missing material) should be directed to the corresponding author for the article.